Journal of Materials Chemistry C

Accepted Manuscript

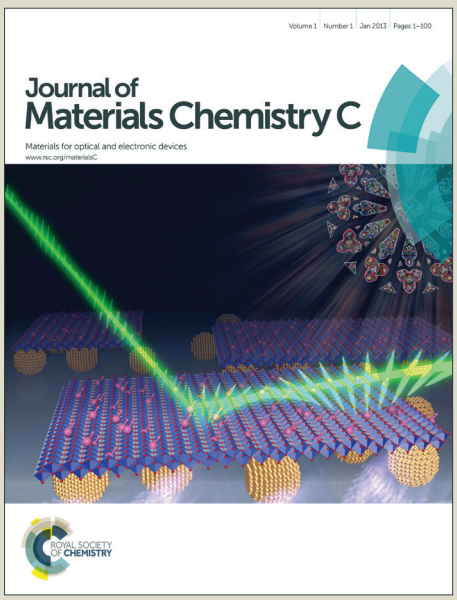

ROYAL SOCIETY OF CHEMISTRY

www.rsc.org/materialsC

Hierarchical SnO_2@NiO core/shell nanoflakearrays as energy-saving electrochromicmaterials

Jia-heng Zhang [a], Jiang-ping Tu [a,b]*, Hong Tang [a], Lu Li [a], Xiu-li Wang [a,b] and Chang-dong Gu [a,b]

a. State Key Laboratory of Silicon Materials, Key Laboratory of Advanced Materials and Applications for Batteries of Zhejiang Province and Department of Materials Science and Engineering, Zhejiang University, Hangzhou 310027, China

b. CyrusTangCenter for Sensor Materials and Applications, Zhejiang University, Hangzhou 310027, China

*Corresponding Author

Tel.: +86 571 87952856. Fax: +86 571 87952573.

E-mail: tujp@zju.edu.cn; tujplab@zju.edu.cn (J.P. Tu)

Abstract

Hierarchical SnO_2@NiO core/shell nanoflake array on FTO-coated glass has been synthesized by a facile two-step solution method toward energy-saving electrochromism. Noticeably, the SnO_2@NiO core/shell nanoflake array film shows a sustained memory effect, which is conducive to saving energy in commercial application. The SnO_2@NiO film exhibits an outstanding electrochromism, including large transmittance modulation (85.3%), fast switching speed (1.7 s and 2.4 s), high coloration efficiency (43.8 cm^2 C^{-1}), excellent reversibility and cycling durability at 550 nm. The enhanced electrochromic performances can be attributed to the unique core/shell architecture, which provides large amounts of active sites for electrochemical reactions, fast ion and electron transfer channels and good strain accommodation ability.

1. Introduction

With the population growing and energy demand increasing, society is faced with two choices: producing more energy or searching the ways to reduce consumption. The former can be solved by burning more fossil fuels but with the worse effects of environmental pollution and resource exhaustion. Therefore the researchers focus on finding the ways to save energy by technology. As a promising energy-savingand environmental protection technology, electrochromic (EC) materials can adjust their optical properties upon applying external voltage, which renders it important applications in the fields of energy-saving smart windows, electronic paper-like displays, eye-glasses, antiglare rear-view mirrors in cars, active camouflage, to name a few.[1−10] Based on function-oriented selection of practical application, it is desirable to synthesize the EC materials with long-term cyclic stability, high coloration efficiency, stable memory effect, large optical modulation and short switching time under a low dc voltage.

Since the discovery of electrochromism, numerous EC materials have been investigated widely, such as transition-metal oxides, conjugated polymers, mixed valence materials, organic molecules, and so forth.[11−16] Among them, NiO is a potential anodic EC material due to its large dynamic range, high electrochromic efficiency and low material cost.[17−21] However, the slow switching speed, poor memory effect and low cycling durability have limited the commercial exploitation of NiO electrochromic film.

As an optical transparent semiconductor with a wide band gap (E_g= 3.6 eV),

SnO_2has been widely applied in solar photovoltaic conversion, window insulation, thermal insulation in lamp, and electrochromic device owing to its high electron mobility (~100–200 cm^2 V^{-1} s^{-1}), chemically inert, stability against atmospheric conditions and high temperature.[22–29] The electrochromism of SnO_2 film has been reported by Orel *et al* [30] and Patil *et al* [31] but with poor electrochromic performances. Currently, the advanced core/shell heterostructures have attracted much attention because of their fascinating synergetic properties or multi-functionalities offered by the composite nanostructures.[32–37] The heterostructure core/shell architecture can make use of the advantages of both components, as well as offer excellent performances through reinforcement or modification of each other. At present, some electrochromic materials with core/shell architecture were reported with excellent electrochromic performance, such as TiO_2/NiO,[19] TiO_2/WO_3,[38] WO_3/polyaniline,[39] and Au/PEDOT.[40] Therefore, it is suggested that integrating NiO and SnO_2 into a core/shell nanostructure array can achieve enhanced electrochromic properties.

In this present work, the hierarchical SnO_2@NiO core/shell nanoflake array is synthesized on FTO (fluorine-doped tin oxide) -coated glass by a simple but powerful two-step solution method. The growth mechanism and electrochromic performances were investigated. Impressively, the SnO_2@NiO core/shell nanoflake array film exhibits enhanced electrochemical performance including large transmittance modulation, more sustained memory effect, fast switching speed, high coloration efficiency and good cycling durability. Due to the large amounts of active sites for electrochemical reactions, fast ion and electron transfer channels and good strain

accommodation ability, the core/shell nanoflake array has potential applications for energy-saving electrochromism.

2. Experimental

2.1 Chemical materials

All solvents and chemicals were of analytical grade without further purification. FTO glass was purchased from Shenzhen Display Photoelectric MaterialCo., Ltd. Tindichloride dehydrate, urea, mercaptoacetic acid, hydrochloric acid (37 wt. %), nickel sulfate, potassium persulfate and aqueous ammonia (25–28%) were purchased from Sinopharm Chemical Reagent Co., Ltd. (China).

2.2 Preparation of SnO_2@NiO core/shell nanoflake arrays

Firstly, SnO_2 nanoflake array was synthesized on FTO-coated glass by a facile hydrothermal method. The experimental details were as follows. 1 g urea, 20 μL mercaptoacetic acid and 1 mL hydrochloric acid (37 wt. %) were dissolved in 80 mL deionized water under magnetical stirring for 1 min in airto form a clear solution, followed by the addition of 0.2 g tindichloride dehydrate. After stirring, the resulting solution was then transferred into a 100 mL Teflon lined stainless steel autoclave, and a clean FTO-coated glass substrate (4×2 cm^2 in size) was submerged in the solution and placed at an angle against the wall of the Teflon lined with the conducting side facing down. Afterwards, the autoclave was heated to 120 ºC in a vacuum oven for 8 h, and cooled down to room temperature under flowing water. After rinsed with deionized water, fully dried in air at 60 ºC, and annealed in a tube furnace at 400 ºC

for 3 h in flowing argon, the SnO_2 nanoflake array was uniformly coated on the FTO glass substrate.

Then, the self-supported SnO_2nanoflake array was used as the scaffold for further NiO growth by a simple chemical bathdeposition (CBD).[41] Solution for CBD was obtained by mixing 0.12 mol $NiSO_4$, 0.0225 mol potassium persulfate and 270 ml de-ionized water in a 500 ml pyrex beaker at 25 ºC. The back side of the as-obtained SnO_2nanoflake array grown on FTO was masked with polyimide tape to prevent the deposition of NiO on the nonconductive side, and then placed vertically in the freshly resulting solution. After adding 30 ml of aqueous ammonia (25–28%), the beaker was kept at room temperature under stirring for 4 min to deposit the precursor film. For comparison, NiO film was also prepared with the same process on bare FTO glass substrate for the same time. After removing the tape masks, the precursor film was rinsed with distilled water and then annealed in a tube furnace at 350 ºC for 1 h in flowing argon after drying.

2.3 Structural characterization

The structure and morphology of the as-prepared films were characterized by X-ray diffraction (XRD, RigakuD/Max-3B), X-ray photoelectron spectroscopy (XPS, Kratos AXIS Ultra DLD), field emissionscanning electron microscopy (FESEM, Hitachi S4800), high-resolution transmission electron microscopy (HRTEM, Tecnai F20) with an X-ray energy dispersive spectroscope (EDS, BRUKER AXS). Raman spectra were recorded by LABRAM HR-800 at an excitation wavelength of 514 nm.

2.4 Electrochemical measurements

A three-electrode cell was used for electrochemical measurements with 1 M KOH aqueous solution as the electrolyte. Cyclic voltammetry (CV) and chronoamperometry (CA) measurements were performed on a CHI660E electrochemical workstation, the platinum foil as the counter electrode and Hg/HgO as the reference electrode.The CV tests of the films were carried out at a scan rate of 20 mV s^{-1} between −0.2 and 0.8 V at 20 ºC. The transmittance spectra of the films in the fully colored and fully bleached states were measured by a SHIMADZU UV-3600 spectrophotometer with wavelength range from 300 to 1000 nm. The memory effects of the EC films were observed under open-circuit voltage conditions.

3. Results and discussion

3.1. Structure and Morphology

The morphologies of bare SnO_2, bare NiO and final SnO_2@NiO core/shell nanoflake arrays on FTO-coated glass are shown in Fig. 1. The panoramic SEM image shows that the SnO_2 nanoflakes are uniformly grown on the substrate (Fig. 1a). The magnified SEM image reveals that the SnO_2 layer is composed of perpendicularly oriented nanoflakes with an average thickness of 20 nm (Fig. 1b). Moreover, the SnO_2 nanoflakes are interconnected with each other to form a hierarchical network. The cross-section SEM image shows the homogeneously aligned SnO_2 nanoflake and that the thickness of the SnO_2 nanoflake layer is about 300 nm. It can be clearly observed that the open space between the NiO nanoflakes is relatively large, with an average thickness of 8 nm and height up to around 200 nm (Fig. 1c and d). After CBD, the

core/shell nanoflake arrays are illustrated in Fig. 1e and f. The nanoflake shells are interconnected but still do not fully cover the entire core. Apparently, the thickness of the whole film increases to about 350 nm, and the surface is covered by numerous leaf-like ultrathin nanoflakes, forming highly porous core/shell architecture. Fig.2 illustrates the two-step synthesis of the SnO_2@NiO core/shell nanoflake array by combining hydrothermal and CBD methods. The hydrothermally synthesized SnO_2 nanoflakes serve as the backbone for the subsequent deposition of NiO. The growth mechanism of the shell structure is due to the "self-assembly" and "oriented attachment" processes. The oriented attachment mechanism refers to the spontaneous self-organization of adjacent particles with a common crystallographic orientation. Subsequently, these particles join into a planar interface. In this work, the SnO_2 nanoflakes act as the backbone, which can guide the self-assembling growth of Ni-based hydroxide nanoparticles in aqueous solution. Then the nanoparticles oriented growth by "oriented attachment". At the beginning of CBD reaction, heterogeneous nucleation occurs when the supersaturated solution is formed with numerous Ni-based hydroxide mesocrystals (NHMs). Then NHMswould attach to the surface of SnO_2 "backbone" to reduce the surface energy with the forming of active nucleation centers. These active sites would minimize the interfacial energy barrier for the subsequent growth of Ni-based hydroxide. At last, NHMs self-assemble, forming the quasi-2D nanoflake structure.[32, 36 42] Generally, the pores or voids between nanoflakes of both the core and shell wouldprovide effective transportation channels for electrons and ions during the electrochromic process. Besides, due to the porous

and ultrathin structure of the core/shell nanoflake arrays, the electrolyte can diffuse into the inside of the electrode materials.[35] Therefore, almost all the active materials could participate in the electrochemical reaction process within a short time, leading to an enhanced electrochromic performance.

The detailed porous core/shell nanoflake structure is further demonstrated by the TEM images. As shown in Fig. 3a, the SnO_2 core nanoflakes have good crystallinity with a thickness of 10−20 nm. The crystalline SnO_2 nanoflakes are covered by a thin and continuous layer, and the outer NiO shell nanoflakes are composed of nanocrystallites with an average thickness of about 8 nm. This unique porous morphological characteristic is favorable for electrolyte penetration and ion/electron fast transfer and may lead to the enhanced electrochemical reactivity. The HRTEM image shown in Fig. 3b (the red box section of Fig. 3a) reveals that the core and shell have distinct set of visible lattice fringes with inter-planar spacing of 0.298 nm and 0.209 nm, corresponding well to the (111) plane of orthorhombic SnO_2 and (200) plane of cubic NiO. The core/shell structure can also be supported by EDS mappings of Ni, Sn and O, as shown in Fig. 3c and d.

The XRD patterns of bare FTO glass, SnO_2nanoflake array, NiO and SnO_2@NiO core/shell nanoflake array films are presented in Fig. 4. For the bare SnO_2 nanoflake array, all the diffraction peaks except the peaks of FTO can be well indexed to orthorhombic SnO_2 phase (JCPDS No. 29-1484).The diffraction peaks of FTO and cubic NiO phase (JCPDS No. 73-1523) can be observed from the pure NiO film. For the SnO_2@NiO core/shell nanoflake array, it can be observed the peaks corresponding

to both NiO and SnO_2. It is worth noting that it is difficult to obtain high intensity peaks of NiO due to the thinness and porous structure of the NiO layer.

In order to further study the surface compositions and chemical states of the SnO_2@NiO core/shell nanoflake array, XPS analysis was conducted in this work. The characteristic peaks of Ni 2p, Sn 3d and O 1s can be observed from the full survey spectrum in Fig. S1a, indicating the existence of NiO and SnO_2. The main peaks of Ni $2p_{3/2}$ spectrum can be deconvoluted into two parts, peak A and B located at 854.1 and 855.9 eV are corresponding to Ni^{2+} and Ni^{3+} respectively, [43, 44] as shown in Fig. S1b. The Ni^{3+} mainly derives from high valence nickel oxides such as $Ni_2O_3{\cdot}H_2O$, β-NiO(OH), or $4Ni(OH)_2{\cdot}NiOOH{\cdot}xH_2O$ due to the effect of persulfate. The O1s spectrum of SnO_2@NiO core/shell nanoflake array film is displayed in Fig. S1c. The O1s peaks mainly include two components, the peaks located at 529.4 and 531.3 eV corresponding to NiO and Ni-OOH bands respectively.[45, 46] The analysis result is in accordance with the analysis of Ni $2p_{3/2}$ spectrum. For the Sn 3d XPS spectrum, as shown in Fig. S1d, the major peaks situated at 486.5 and 495.0 eV are corresponding to Sn $3d_{5/2}$ and Sn $3d_{3/2}$.[47] Due to the ultrathin and porous NiO shells coated uniformly on the SnO_2 cores, the Sn 3d XPS spectrum is observable but very rough.

3.2. Electrochemical and Electrochromic Performances

The electrochromic performances of the SnO_2@NiO core/shell nanoflake array were evaluated using CV measurements. Fig. 5 compares the CV curves of bare SnO_2, bare NiO and SnO_2@NiO films carried out in 1 M KOH solution within the potential region of −0.2− 0.8 V at a scan rate of 20 mV s^{-1} for the 10th cycle. The CV curve of

the bare SnO_2 film is almost a straight line, and no redox peak appears. Only one redox couple of NiO is observed for both the bare NiO and SnO_2@NiO films, indicating that the NiO plays significant role for electrochromism and the SnO_2 plays the role of scaffold. The anodic/cathodic peaks are assigned to the conversion between NiO and NiOOH, and the involved reactions in the alkaline electrolyte can be simply illustrated as follows:

$$NiO + OH^- \leftrightarrow NiOOH + e^- \quad (1)$$

The films are colored and bleached reversibly with the OH^- ions inserting and deserting, because of the transformation between Ni^{3+} and Ni^{2+} (the insets of Fig. 5). It is generally known that highly symmetrical redox couple peaks mean good reversibility andthe potential separation of redox peaks is used as a measure of reversibility.[41, 48] The SnO_2@NiO film has a lower oxidation potential comparing with the bare NiO, as well as a lower reduction potential. The potential separations are almost same for both the films,indicating that the SnO_2@NiO films has the same good reversibility as the bare NiO. It is obviously observed that the onset potential of the oxidation peak of the SnO_2@NiO core/shell nanoflake array film shifts negatively, compared to that of the bare NiO. What's more, the current densities of the redox couple peaks for the SnO_2@NiO core/shell nanoflake array film are much higher than those of the bare NiO. The negative shifts indicate that the SnO_2@NiO film would require a smaller energy barrier for the reaction of NiO → NiOOH, meanwhile indicate the improvement in the electrochemical activities and reaction kinetics of the NiO. The higher current density of the SnO_2@NiO film indicates that more active

materials participate in the electrochromic reaction within a certain period of time, which can also show the enhancement in the electrochemical activities and reaction kinetics. EIS is a well-developed technique, usually applied to determine the ion diffusion and charge-transfer properties. The enhanced reaction kinetics of the electrochromic films is also supported by EIS at fully discharge state at 10th cycle. Fig. S2 shows the Nyquist plots of the bare NiO and SnO_2@NiO films. It is well accepted that the semicircle in the high-medium frequency range corresponds to charge-transfer resistance, and the low-frequency line represents Warburg impedance related to ion diffusion between the electrode and electrolyte. It can be observed that the semicircle of the SnO_2@NiO film is smaller than that of the bare NiO film, which means a smaller charge-transfer resistance. The slope of inclined line for the SnO_2@NiO film is gentle than that of the bare NiO film, signifying a higher ion-diffusion rate. The lower resistance and higher ion-diffusion rate of SnO_2@NiO film mean a faster charge-transfer process and better electrolyte accessibility.[41.49, 50] The enhanced electrochemical activities and reaction kineticscan be attributed to the unique porous architecture of SnO_2@NiO film, which is favorable for electrolyte penetration and ion/electron fast transfer.

In order to further verify the proposed reaction $NiO + OH^- \leftrightarrow NiOOH + e^-$, the Ni 2p XPS spectra of the SnO_2@NiO core/shell nanoflake array film in both colored state (0.8 V) and bleached state (−0.2 V) were conducted. The intensity ratio of peak B/peak A increases obviously after coloration (Fig. 6a), which supports the transformation from NiO to NiOOH. The Raman spectra of SnO_2@NiO core/shell

nanoflake array film in bleached and colored states prove the formation of NiOOH, as displayed in Fig. 6b. For the bleached film, the observed bands centered at 561 and 1090 cm^{-1} could be assigned to the first (LO) and the second (2LO) longitudinal optical modes of NiO, respectively. [51−53] The primarily two bands at around 472 and 778 cm^{-1} are corresponding to SnO_2 vibration modes of E_g and B_{2g}, respectively. [54−56] Then the film was cycled with a step voltage of 0.8 V to reach the colored state. The characteristic spectrum of NiOOH can be observed, exhibiting a couple of strong bands at 473 and 555 cm^{-1} attributed to stretching vibrational modes involving [Ni^{3+}=O] and [Ni^{3+}–O] sites, respectively.[57, 58] From the above experimental results, it is believed that the film iscolored with the formation of NiOOH and the proposed reaction mechanism is reasonable.

The optical transmittance measurements are conducive in analysis the stability, reversibility, persistency, and switching response of the SnO_2@NiO core/shell nanoflake array film. The transmittance spectra are measured in the colored and bleached states from 300 nm to 1000 nm, as presented in Fig. 7. The NiO and SnO_2@NiO film electrodes are colored by applying step voltages of 0.8 V for coloration and −0.2 V for bleaching (vs. Hg/HgO). As seen in this figure, The SnO_2@NiO core/shell nanoflake array film presents a noticeable electrochromism with variation of transmittance up to 85.3 % at 550 nm, while the bare NiO film reaches only about 75.8 %. The enhanced optical modulation is larger than most of NiO electrochromic films in previously reportedworks.[17, 20, 59−62] In addition, we also conduct the transmittance measurement of the bare SnO_2 film in the potential region

of −0.2− 0.8 V, as shown in Fig. S3. There is no obvious change with color when a voltage is applied, indicating that the high transparency SnO_2 layer has no synergistic effect with NiO for electrochromism.

With such promising results, the CA (between −0.2 and 0.8 V) and the corresponding in situ transmittance measurements are employed to study the switching time characteristics of the films, as displayed in Fig. 9. The coloration and bleaching times are defined as the time required for a 90% change in the whole transmittance modulation at a wavelength. The SnO_2@NiO core/shell nanoflake array film exhibits fast coloration and bleaching times for 1.7 s and 2.4 s respectively, while the bare NiO film needs 3.2 s and 5.0 s. To our knowledge, the switching times of SnO_2@NiO core/shell nanoflake arrays are faster than most other nanostructured NiO films, such as NiO nanoflake (8 s and 10 s),[63] NiO octahedral-like nanoparticle (7.4 s and 6.5 s),[20] NiO dandelion flower-like nanosphere (5.84 s and 4.43 s),[62] NiO nanowall (3 s and 4 s),[64] NiO nanorice (4.2 s and 2.4 s),[65] NiO hexagonal nanoplate (26.4 s and 44 s), [61] and porous NiO/reduced graphene oxide hybrid film (7.2 s and 6.7 s).[66] The fast switching speed of the SnO_2@NiO core/shell nanoflake array film can be ascribed to the unique porous architecture including the SnO_2 nanoflake core, NiO nanoflake shell, and ordered array configuration. The highly porous structure shortens the transportation/diffusion path of both electrons and ions, promotes the efficient contact between electrolyte and the active materials, and provides more active sites for electrochemical reactions. The result is coincident with the result of CV measurements.

The coloration efficiency (*CE*) is a key parameter for the comparison of various electrochromic materials,[67] which is evaluated through thefollowing equations:

$$CE(\lambda) = \frac{\Delta OD(\lambda)}{Q} \quad (2)$$

$$\Delta OD(\lambda) = \log \frac{T_b}{T_c} \quad (3)$$

$$Q = \int_{t1}^{t2} j(t)dt \quad (4)$$

Where ΔOD is the chance of optical density at a wavelength, calculated from the transmittances of the bleached (T_b) and colored (T_c) states; Q is the total inserted (or extracted) charge during the coloring period. An ideal electrochromic material should maximize its *CE*, demanding a large modulation range of transmittance induced by a small amount of charge.[5] Based on these equations, the calculated value of *CE* for SnO_2@NiO core/shell nanoflake array filmis as high as 43.75 $cm^2\ C^{-1}$, while that of the bare NiO film is only 32.39 $cm^2\ C^{-1}$ (Fig. S4). The enhanced *CE* value is a direct consequence of the core/shell porous structure providing good ion access and a larger modulation range of transmittance.

The memory effect refers to that the momentary state of coloration remains unchanged when the applied voltage is removed during the switchof coloration.[68–70] Fig. 8 shows the transmittance of the coloured bare NiO and SnO_2@NiO core/shell nanoflake array films after aging in air for different time. The colored transmittance gradually increased with the time for both the filmsunder open-circuit conditions. It is obviouslyobserved that the transmittance of the SnO_2@NiO film increases more slowly than that of the bare NiO. After 48 h, the transmittance of SnO_2@NiO and bare

NiO film increased 11.2 % and 58.7 % at 550 nm, respectively. The transmittance of the formerstill maintained at 32.5 % even for 144 h, while the latter at 85.7 %, almost equivalent to the bleached state (shown in the insets of Fig. 8). The SnO_2@NiO core/shell nanoflake array film has a good memory effect under open-circuit conditions, and electrical energy is only required during switching, and not for maintaining the constant state of coloration. A memory loss occurs when the inserted charge is removed from the EC film. On the one hand, the self-discharge process of the incorporated protons might be affected by the structural characteristics of electrode. The porous structure could give substantial enhancements in charge storing, suppressing the self-discharge of the inserted charge.[71–73] On the other hand, the open circuit voltage (OCV) of the SnO_2@NiO is measuredto be 0.54 V, which is lower than that (0.58 V) of the bare NiO. The lower OCV would hinder the self-discharge of the inserted charge.[74] Therefore, the SnO_2@NiO film exhibits a good memory effect than the bare NiO film. It is believed that the property of energy-saving would promote the application of the SnO_2@NiO core/shell nanoflake array film in the field of electrochromism.

The cycling durability of the bare NiO and SnO_2@NiO core/shell nanoflake array electrodes is performed within a 2200 cycles test (Fig. 10). After 800 cycles, the modulation ranges of the bare NiO and SnO_2@NiO films decayed to about 4.8 % and 65.7 % respectively. Furthermore, even subjected to 2200 cycles, the transmittance modulation of SnO_2@NiO film could still maintain 51.5 %. In addition, after 2200 cycles, the SnO_2/NiO core/shell nanoflake array can effectively keep the structure

stable except that the nanoflakes become a little thinner, as shown in Fig. S5. The enhanced cycling durability can be possibly attributed to that the porous core/shell array configuration can reduce internal strain and accommodate the vast volume changes.[32, 33, 35, 37]

4. Conclusions

We have demonstrated a simple and facile solution method for the direct growth of hierarchical SnO_2@NiO core/shell nanoflake array on FTO-coated glass toward energy-saving electrochromism. In this core/shell structure, the SnO_2 nanoflake core is coated with a shell of NiO nanoflakes, exhibiting a porous morphology. The core/shell nanoflake array film exhibits excellent electrochromic performances with large transmittance modulation, sustained memory effect, fast switching speed, high coloration efficiency and good cycling durability. These enhanced electrochromic performances can be attributed to the unique porous and conductive, core/shell, and array architecture. In view of the noticeable electrochromic performances, it is appreciable that the hierarchical SnO_2@NiO core/shell nanoflake array would promote the commercialization of NiO based energy-saving electrochromic film.

Acknowledgments

This work was supported by the Program for Innovative Research Team in University of Ministry of Education of China (IRT13037), the Key Science and Technology Innovation Team of Zhejiang Province (2010R50013) and a support program of the Ministry of Education of China.

References

1. C. Y. Yan, W. B. Kang, J. X. Wang, M. Q. Cui, X. Wang, C. Y. Foo, K. J. Chee and P. S. Lee, *ACS Nano*, **2013**, 8, 316.
2. B. Baloukas, J. M. Lamarre and L. Martinu, *Solar Energy Mater. Solar Cells*, **2011**, 95, 807.
3. D. S. Dalavi, R. S. Devan, R. S. Patil, Y. R. Ma, M. G. Kang, J. H. Kim and P. S. Patil, *J. Mater. Chem. A*, 2013, **1**, 1035.
4. G. A. Niklasson and C. G. Granqvist, *J. Mater. Chem.*, **2007**, 17, 127.
5. M. R. J. Scherer and U. Steiner, *Nano Lett.*, **2012**, 13, 3005.
6. J. W. Liu, J. Zheng, J. L. Wang, J. Xu, H. H. Li and S. H. Yu, *Nano Lett.*, **2013**, 13, 3589.
7. D. D. Yao, R. A. Rani, A. P. O'Mullane, K. Kalantar-zadeh and J. Z. Ou, *J. Phys. Chem. C*, **2013**, 118, 476.
8. Z. Xie, X. J. Jin, G. Chen, J. Xu, D. Chen and G. Z. Shen, *Chem. Commun.*, **2014**, 50, 608.
9. M. V. Nguyen, D. Kim and H. Kim, *J. Mater. Chem. C*, 2013, **1**, 3399.
10. H. Z. Li, G. Y. Shi, H. Z. Wang, Q. H. Zhang and Y. Q. Li, *J. Mater. Chem. A*, **2014**, 2, 11305.
11. K. W. Weng, Y. C. Chen, T. N. Lin, Y. D. Li and T. L. Chen, *Vacuum*, **2013**, 87, 169.
12. Y. Zhang, S. H. Lee, A. Mascarenhas and S. K. Deb, *Appl. Phys. Lett.*, **2008**, 93, 203508.
13. X. H. Xia, D. L. Chao, X. Y. Qi, Q. Q. Xiong, Y. Q. Zhang, J. P. Tu, H. Zhang and H. J. Fan, *Nano Lett.*, **2013**, 13, 4562.
14. J. Z. Chen, W. Y. Ko, Y. C. Yen, P. H. Chen and K. J. Lin, *ACS Nano*, **2012**, 6, 6633.
15. B. Kattouf, Y. Ein-Eli, A. Siegmann and G. L. Frey, *J. Mater. Chem. C,* **2013**, 1, 151
16. D. Navarathne and W. G. Skene, *J. Mater. Chem. C,* **2013**, 1, 6743.
17. F. Lin, D. Nordlund, T. C. Weng, D. Sokaras, K. M. Jones, R. B. Reed, D. T. Gillaspie, D. G. J. Weir, R. G. Moore, A. C. Dillon, R. M. Richards and C. Engtrakul, *ACS Appl. Mater. Interfaces*, **2013**, 5, 3643.
18. G. F. Cai, C. D. Gu, J. Zhang, P. C. Liu, X. L. Wang, Y. H. You and J. P. Tu, *Electrochim. Acta*, **2013**, 87, 341.
19. G. F. Cai, J. P. Tu, D. Zhou, L. Li, J. H. Zhang, X. L. Wang and C. D. Gu, *J. Phys. Chem. C*, **2014**, 118, 6690.

20. J. Y. Liu, Y. Ren, B. Dasgupta, H. Tanoto, H. L. Seng, W. K. Chim, S. F. Y. Li and S. Y. Chiam, *J. Mater. Chem. A*, 2013, **1**, 15095.

21. J. H. Zhang, G. F. Cai, D. Zhou, H. Tang, X. L. Wang, C. D. Gu and J. P. Tu, *J. Mater. Chem. C*, **2014**, 2, 7013.

22. K. K. Purushothaman, M. Dhanasankar, G. Muralidharan, *Surf. Rev. Lett.*, **2007**, *14*, 1149.

23. C. E. Benouis, M. Benhaliliba, Z. Mouffak, A. Avila-Garcia, A. Tiburcio-Silver, M. Ortega Lopez, R. Romano Trujillo and Y. S. Ocak, *J. Alloys Compd.*, **2014**, 603, 213.

24. L. Zhang, G. Q. Zhang, H. B. Wu, L. Yu and X. W. Lou, *Adv. Mater.*, **2013**, 25, 2589.

25. J. S. Chen, M. F. Ng, H. B. Wu, L. Zhang and X. W. Lou, *CrystEngComm*, **2012**, 14, 5133.

26. J. G. Kim, S. H. Nam, S. H. Lee, S. M. Choi and W. B. Kim, *ACS Appl. Mater. Interfaces*, **2011**, 3, 828.

27. Y. L. Wang, J. J. Xu, H. Wu, M. Xu, Z. Peng and G. F. Zheng, *J. Mater. Chem.*, **2012**, 22, 21923.

28. L. Zhang, H. B. Wu and X. W. Lou, *Mater. Horizons*, **2014**, 1, 133.

29. X. C. Dou, R. R. Prabhakar, N. Mathews, Y. M. Lam and S. Mhaisalkar, *J. Electrochem. Soc.*, **2012**, 159, H735.

30. B. Orel, U. Lavrenčič-Štangar and K. Kalcher, *J. Electrochem. Soc.*, **1994**, 141, L127.

31. P. S. Patil, S. B. Sadale, S. H. Mujawar, P. S. Shinde and P. S. Chigare, *Appl. Surf. Sci.*, **2007**, 253, 8560.

32. X. H. Xia, J. P. Tu, Y. Q. Zhang, X. L. Wang, C. D. Gu, X. B. Zhao and H. J. Fan, *ACS Nano*, **2012**, 6, 5531.

33. J. B. Wu, Z. G. Li, X. H. Huang and Y. Lin, *J. Power Sources*, **2013**, 224, 1.

34. L. Huang, D. C. Chen, Y. Ding, Z. L. Wang, Z. Z. Zeng and M. L. Liu, *ACS Appl. Mater. Interfaces*, **2013**, 5, 11159.

35. X. Y. Liu, S. J. Shi, Q. Q. Xiong, L. Li, Y. J. Zhang, H. Tang, C. D. Gu, X. L. Wang and J. P. Tu, *ACS Appl. Mater. Interfaces*, **2013**, 5, 8790.

36. L. Q. Mai, F. Yang, Y. L. Zhao, X. Xu, L. Xu and Y. Z. Luo, *Nat. Commun.*, **2011**, 2, 5.

37. X. H. Xia, J. P. Tu, Y. Q. Zhang, J. Chen, X. L. Wang, C. D. Gu, C. Guan, J. S. Luo and H. J. Fan, *Chem. Mater.*, **2012**, 24, 3793.

38. G. F. Cai, D. Zhou, Q. Q. Xiong, J. H. Zhang, X. L. Wang, C. D. Gu and J. P. Tu, *Solar*

Energy Mater. Solar Cells, **2013**, 117, 231.

39. G. F. Cai, J. P. Tu, D. Zhou, J. H. Zhang, X. L. Wang and C. D. Gu, *Solar Energy Mater. Solar Cells*, **2014**, 122, 51.
40. T. Augusto, É. Teixeira Neto, Â. A. Teixeira Neto, R. Vichessi, M. Vidotti and S. I. C. de Torresi, *Solar Energy Mater. Solar Cells*, **2013**, 118, 72.
41. X. H. Xia, J. P. Tu, J. Zhang, X. L. Wang, W. K. Zhang and H. Huang, *Electrochim. Acta*, **2008**, 53, 5721.
42. R. L. Penn and J. F. Banfield, *Science*, **1998**, 281, 969.
43. P. Dufresne, E. Payen, J. Grimblot and J. P. Bonnelle, *J. Phys. Chem.*, **1981**, 85, 2344.
44. K. K. Lian, D. W. Kirk and S. J. Thorpe, *J. Electrochem. Soc.*, **1995**, 142, 4309.
45. C. E. Dubé, B. Workie, S. P. Kounaves, A. Robbat, M. L. Aksub and G. Davies, *J. Electrochem. Soc.*, **1995**, 142, 3357.
46. Y. J. Mai, J. P. Tu, X. H. Xia, C. D. Gu and X. L. Wang, *J. Power Sources*, **2011**, 196, 6388.
47. L. Yan, J. S. Pan and C. K. Ong, *Mater. Sci. Eng. B*, **2006**, 128, 34.
48. L. L. Zhao, G. Su, W. Liu, L. X. Cao, J. Wang, Z. Dong and M. Q. Song, *Appl. Surf. Sci.*, **2011**, 257, 3974.
49. X. H. Xia, Z. Y. Zeng, X. L. Li, Y. Q. Zhang, J. P. Tu, N. C. Fan, H. Zhang and H. J. Fan, *Nanoscale*, **2013**, 5, 6040.
50. G. F. Cai, X. L. Wang, D. Zhou, J. H. Zhang, Q. Q. Xiong, C. D. Gu and J. P. Tu, *RSC Adv.*, **2013**, 3, 6896.
51. A. C. Gandhi, J. Pant, S. D. Pandit, S. K. Dalimbkar, T. S. Chan, C. L. Cheng, Y. R. Ma and S. Y. Wu, *J. Phys. Chem. C*, **2013**, 117, 18666.
52. M. Marciuš, M. Ristić, M. Ivanda and S. Musić, *J. Alloys Compd.*, **2012**, 541, 238.
53. G. M. Zhou, D.W. Wang, L. C. Yin, N. Li, F. Li and H. M. Cheng, *ACS Nano*, **2012**, 6, 3214.
54. B. Mallesham, P. Sudarsanam, G. Raju and B. M. Reddy, *Green Chem.*, **2013**, 15, 478.
55. F. H. Aragón, J. A. H. Coaquira, P. Hidalgo, S. W. da Silva, S. L. M. Brito, D. Gouvêa and P. C. Morais, *J. Raman Spectroscopy*, **2011**, 42, 1081.
56. C. S. Xiong, Y. H. Xiong, H. Zhu, Y. H. Zhang and Y. L. Liu, *Sci. China Ser. A-Math.*, **1997**, 40, 1222.
57. B. S. Yeo and A. T. Bell, *J. Phys. Chem. C*, **2012**, 116, 8394.

58. Y. L. Lo and B. J. Hwang, *Langmuir*, **1998**, 14, 944.

59. S. Pereira, A. Gonçalves, N. Correia, J. Pinto, L. Pereira, R. Martins and E. Fortunato, *Solar Energy Mater. Solar Cells*, **2014**, 120, Part A, 109.

60. R. A. Patil, R. S. Devan, J.-H. Lin, Y.-R. Ma, P. S. Patil and Y. Liou, *Solar Energy Mater. Solar Cells*, **2013**, 112, 91.

61. D. Y. Ma, G. Y. Shi, H. Z. Wang, Q. H. Zhang and Y. G. Li, *Nanoscale*, **2013**, 5, 4808.

62. D. S. Dalavi, R. S. Devan, R. S. Patil, Y.-R. Ma, M.-G. Kang, J.-H. Kim and P. S. Patil, *J. Mater. Chem. A*, **2013**, 1, 1035.

63. X. H. Xia, J. P. Tu, J. Zhang, X. L. Wang, W. K. Zhang and H. Huang, *Solar Energy Mater. Solar Cells*, **2008**, 92, 628.

64. Z. Chen, A. Xiao, Y. Chen, C. Zuo, S. Zhou and L. Li, *J. Phys. Chem. Solids*, **2013**, 74, 1522.

65. C. C. Liao, *Solar Energy Mater. Solar Cells*, **2012**, 99, 26.

66. G. F. Cai, J. P. Tu, J. Zhang, Y. J. Mai, Y. Lu, C. D. Gu and X. L. Wang, *Nanoscale*, **2012**, 4, 5724.

67. J. Deng, X. K. Fu, G. Wang, L. Wu and J. Huang, *Electrochim. Acta*, **2012**, 85, 195.

68. S. Y. Lin, Y. C. Chen, C. M. Wang, C. Y. Wen and T. Y. Shih, *Solid State Ionics*, **2012**, 212, 81.

69. Y. C. Nah, K. S. Ahn and Y. E. Sung, *Solid State Ionics*, **2003**, 165, 229.

70. H. J. Yen, C. J. Chen and G. S. Liou, *Adv. Funct. Mater.*, **2013**, 23, 5307.

71. H. S. Shim, J. W. Kim, Y.E. Sung and W. B. Kim, *Solar Energy Mater. Solar Cells*, **2009**, 93, 2062.

72. Z. Yu, J. H. Du and C. A. Li, *Proc. SPIE 3560, Display Devices and Systems II,* vol. 152, **1998**; pp 152.

73. A. Gonçalves, C. Costa, S. Pereira, N. Correia, M. M. Silva, P. C. Barbosa, L. C. Rodrigues, I. Henriques, R. Martins and E. Fortunato, *Polym. Adv. Technol.*, **2012**, 23, 791.

74. H. J. Ahn, H. S. Shim, Y. E. Sung, T. Y. Seong and W. B. Kim, *Electrochem. Solid-State Lett.*, **2007**, 10, E27.

Figure captions

Fig. 1 SEM images of the films: (a, b) SnO_2, (c, d) NiO and(e, f)SnO_2@NiO (cross sectional view presented in inset).

Fig. 2 Schematic illustration of the two-step facile synthesis method of SnO_2@NiO core/shell nanoflake arrays on FTO-coated glass.

Fig. 3 TEM images of (a, b) SnO_2@NiO core/shell nanoflake and (c, d) corresponding EDS mapping.

Fig. 4 XRD patterns of bare FTO,bare SnO_2, bare NiO and SnO_2@NiO core/shell nanoflake array films.

Fig. 5 The 10th CV curves of the SnO_2,NiO and SnO_2@NiO films at a scan rate of 20 mV s^{-1}

Fig. 6 (a) Ni $2p_{3/2}$ XPS and (b) Raman spectra of SnO_2@NiO core/shell nanoflake array film in both bleached and colored states.

Fig. 7 Optical transmittance spectra of the NiOand SnO_2@NiO films from 300 to 1000 nm.

Fig. 8 (a) CA with voltage interval from −0.2 V to 0.8 V, and (b) the corresponding transmittance in situ of the NiOand SnO_2@NiO films at 550 nm

Fig. 9 The memory effect tests of the (a) NiO and (b) SnO_2@NiO films.

Fig. 10 Durability tests of the NiOand SnO_2@NiO films for 2200 cycles at 550 nm. (SEM images of SnO_2@NiO film after 2200 cycles in insets)

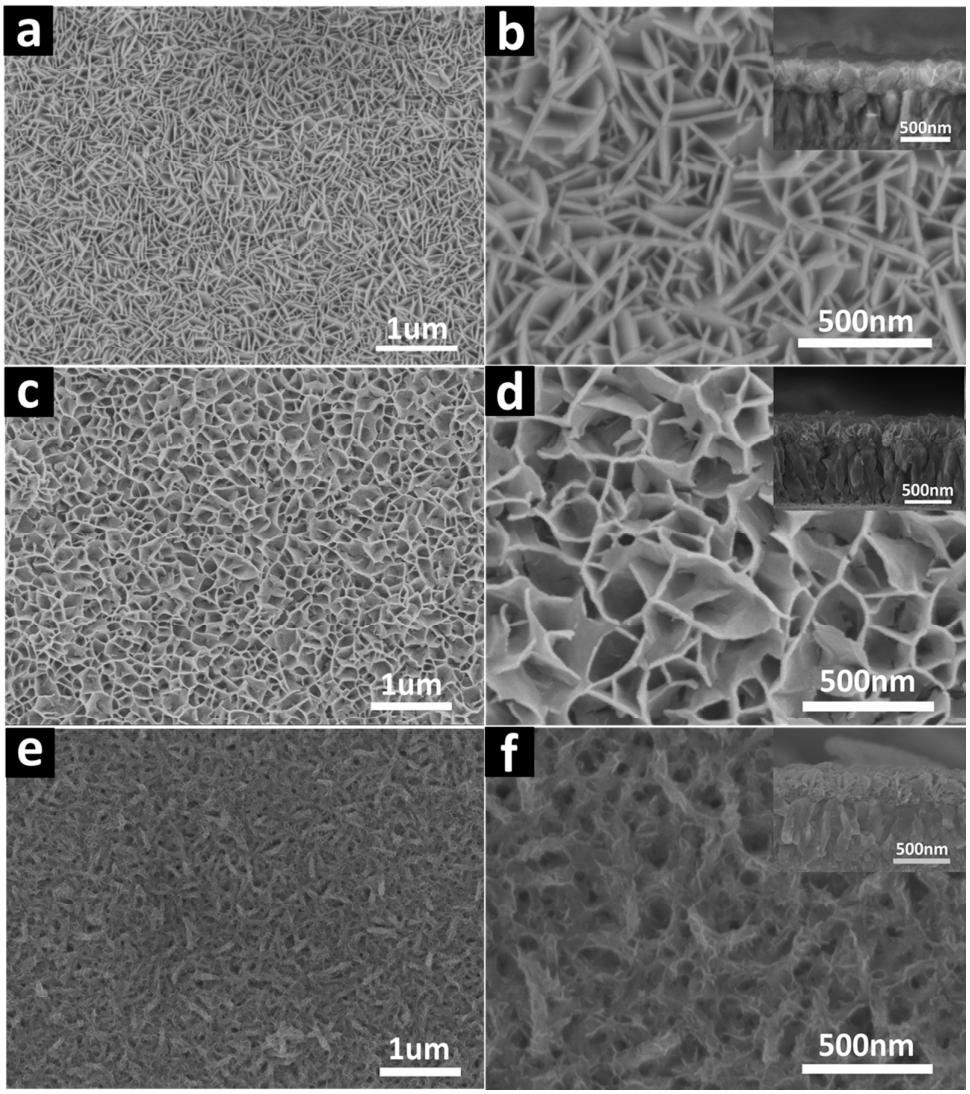

Fig. 1

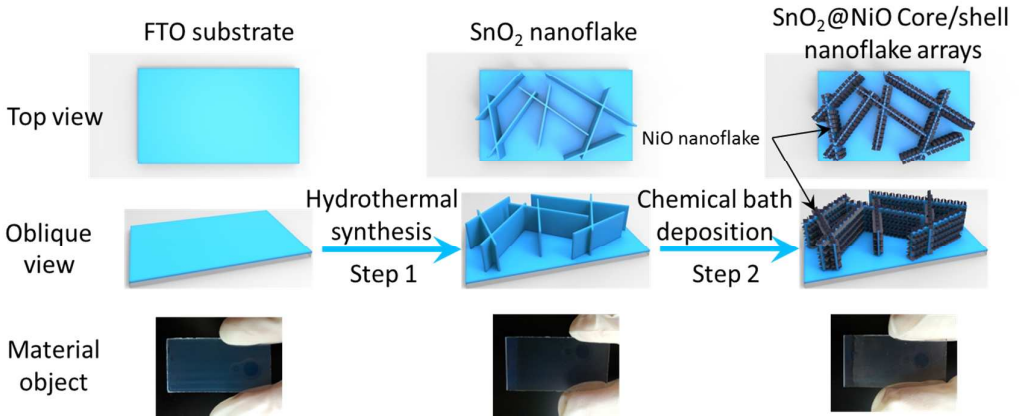

Fig. 2

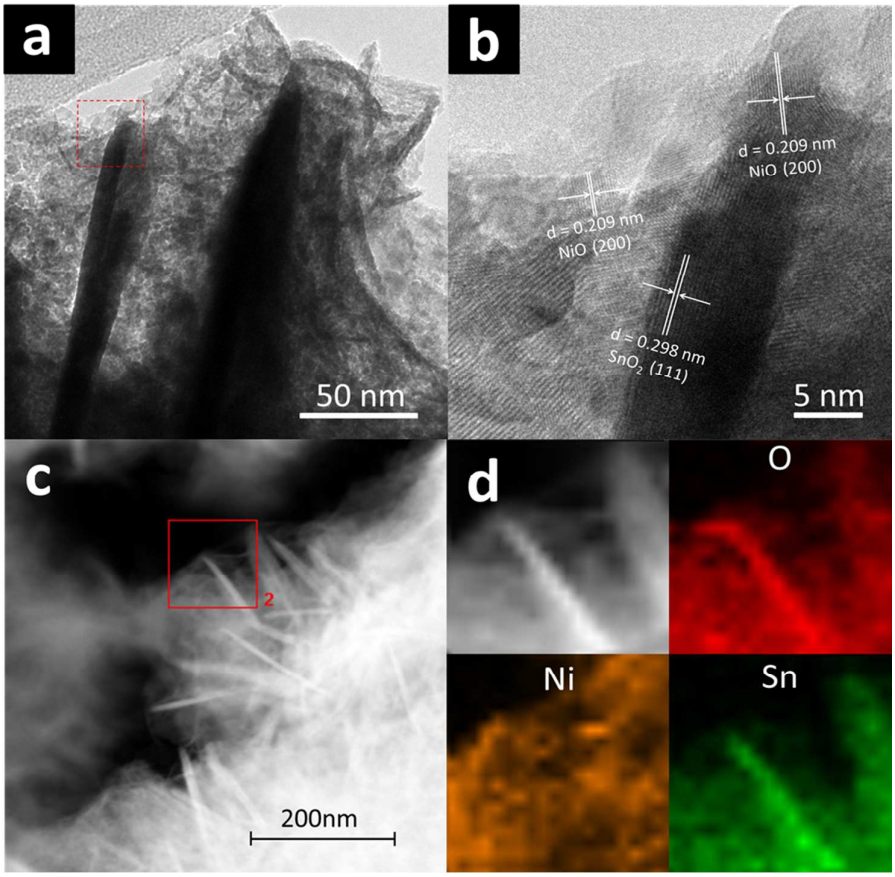

Fig. 3

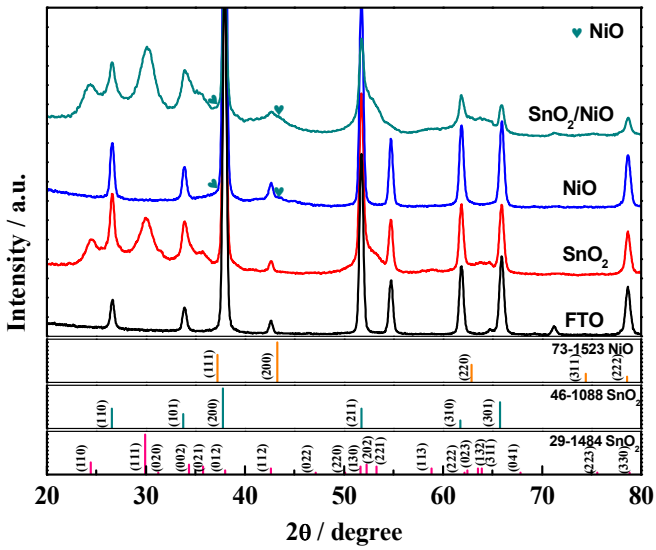

Fig. 4

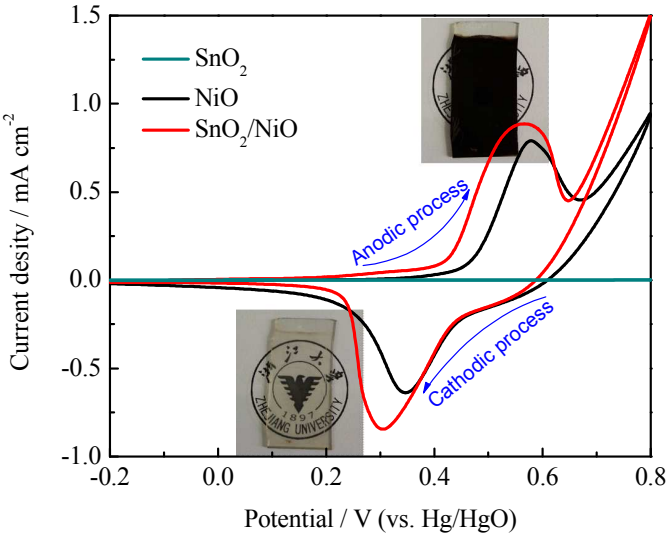

Fig. 5

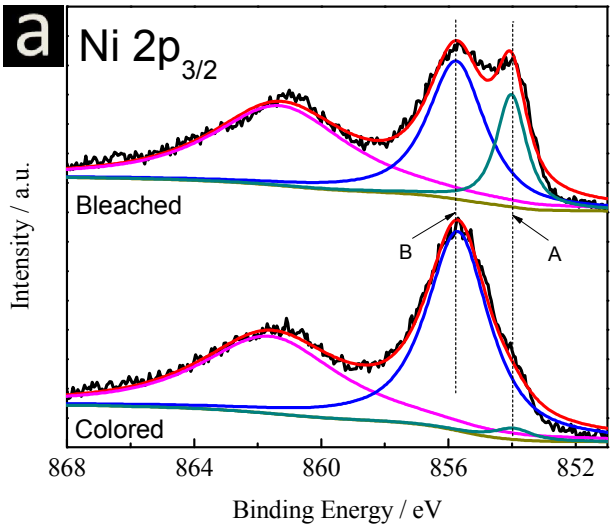

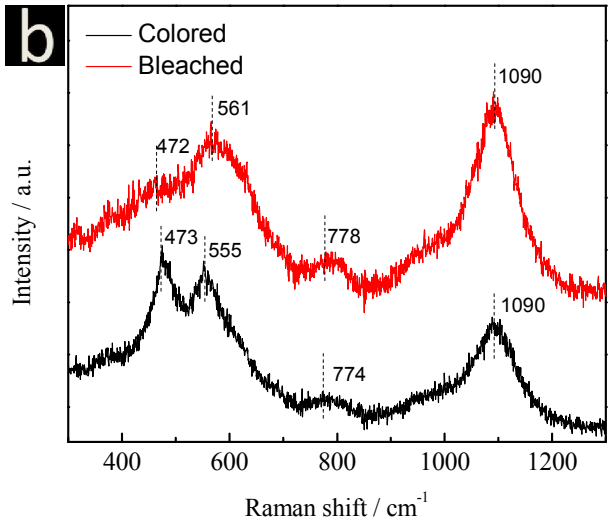

Fig. 6

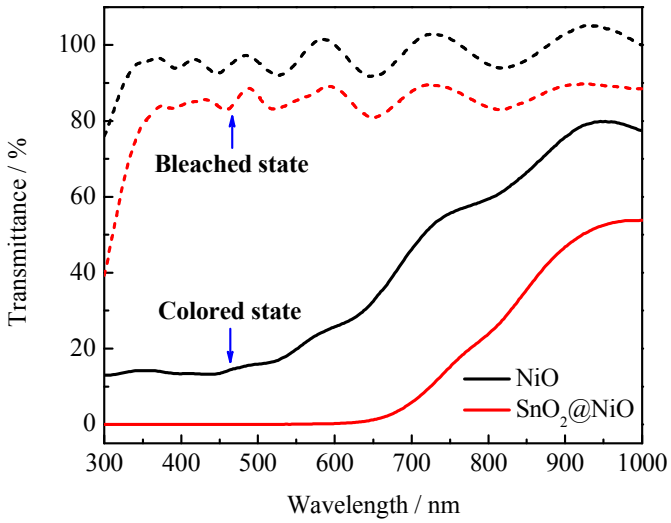

Fig. 7

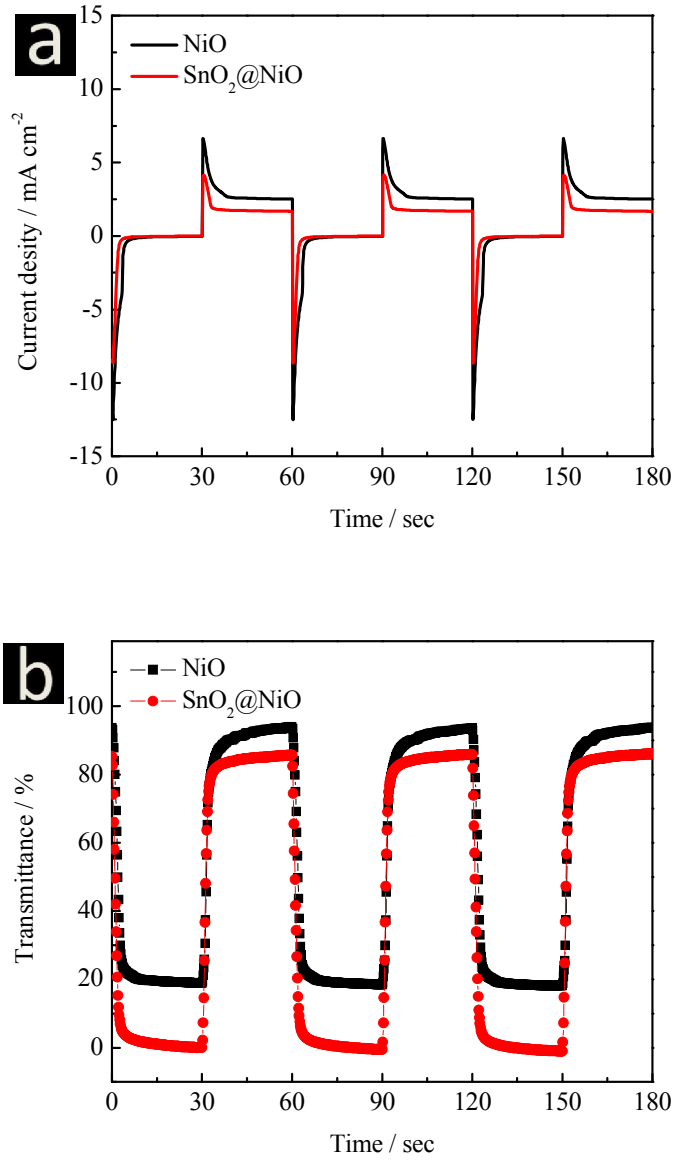

Fig. 8

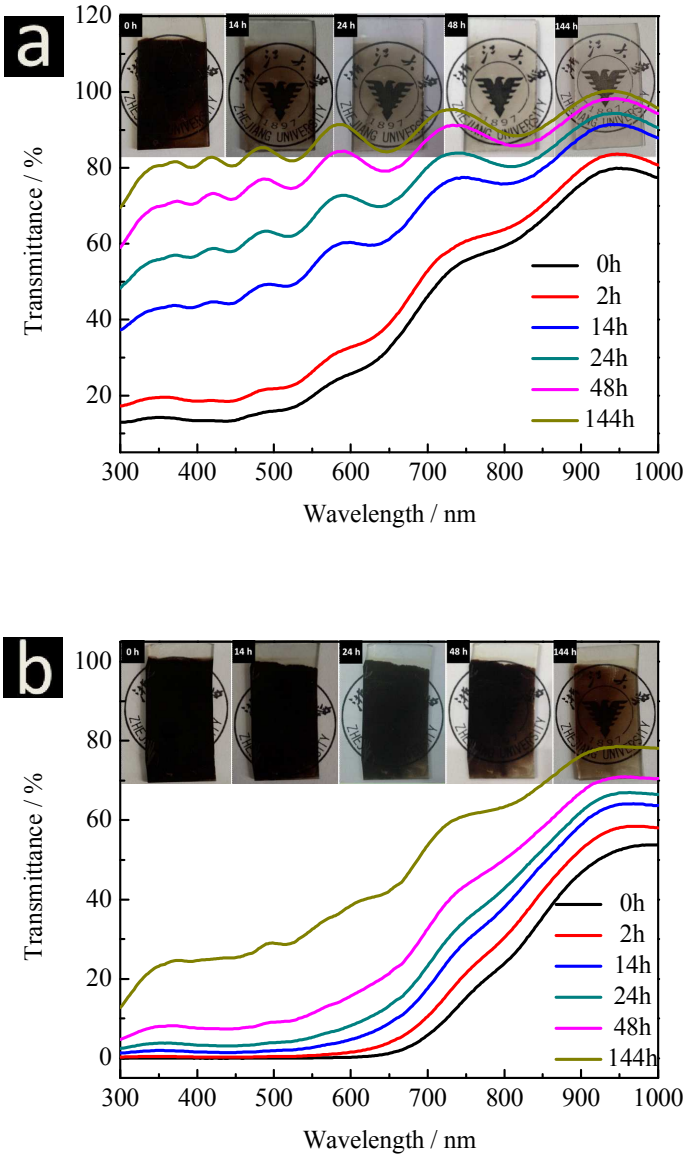

Fig. 9

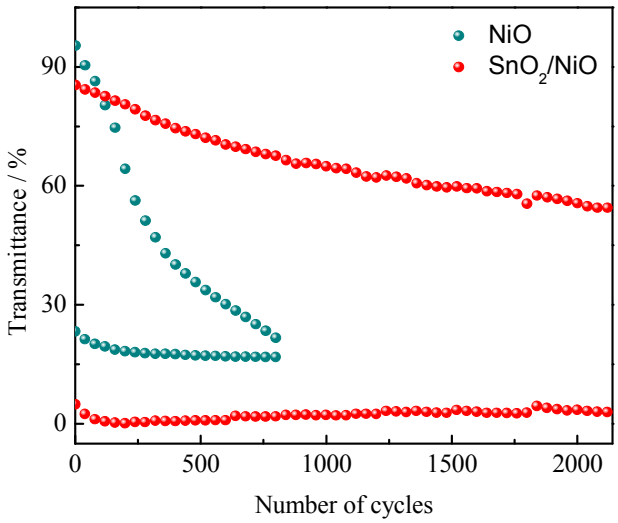

Fig. 10

Table of Content

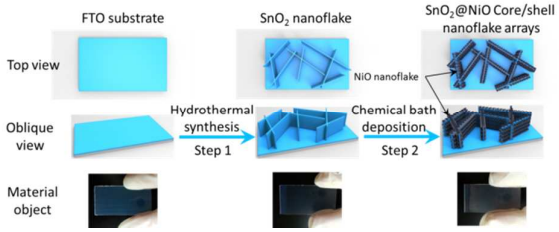

Hierarchical SnO_2@NiO core/shell nanoflake arrays on FTO have been synthesized by a facile solution-based method toward excellent energy-saving electrochromism.